Submitted to small NANO MICRO

DOI: 10.1002/smll.((smll.201202843))

Cell Surface Receptor Targeted Biomimetic Apatite Nanocrystals for Cancer Therapy

*Michele Iafisco, Josè Manuel Delgado-Lopez, Elena Maria Varoni, Anna Tampieri, Lia Rimondini, Jaime Gomez-Morales, and Maria Prat**

[*] Dr. M. Iafisco,[+][++] Dr. E. M. Varoni,[++] Prof. L. Rimondini, Prof. M. Prat
Università del Piemonte Orientale
Dipartimento di Scienze della Salute
Via Solaroli 17, 28100 Novara, Italy
E-mail:mprat@med.unipmn.it
Dr. J. M. Delgado-Lopez,[++] Dr. J. Gomez-Morales
IACT (CSIC-UGR)
Laboratorio de Estudios Cristalográficos,
Av. Las Palmeras 4, E-18100 Armilla, Spain
E-mail: jaime@lec.csic.es
Dr. A. Tampieri
National Research Council (CNR)
Institute of Science and Technology for Ceramics (ISTEC)
Via Granarolo 64, 48018 Faenza (RA), Italy
Prof. L. Rimondini, Prof. M. Prat
Centro di Biotecnologie per la Ricerca Medica Applicata (BRMA)
Via Solaroli 17, 28100 Novara, Italy
Laboratorio de Estudios Cristalográficos,
Av. Las Palmeras 4, E-18100 Armilla, Spain
E-mail: mprat@med.unipmn.it
[+] Current address:
National Research Council (CNR)
Institute of Science and Technology for Ceramics (ISTEC)
Via Granarolo 64, 48018 Faenza (RA), Italy
[++] M. I., J. M. D.-L. and E. M. V. have contributed equally to this work.

Supporting Information is available on the WWW under http://www.small-journal.com or from the author.

Keywords: drug delivery, *in vitro* assays, active cancer cells targeting, apatite nanoparticles, monoclonal antibody

Nanosized drug carriers functionalized with moieties specifically targeting tumor cells are promising tools in cancer therapy, due to their ability to circulate in the bloodstream for

longer periods and to their selectivity for tumor cells, enabling to spare healthy tissues. Because of its biocompatibility, high bioresorbability and responsiveness to pH changes, synthetic biomimetic nanocrystalline apatites were used as nanocarriers to produce multifunctional nanoparticles, by coupling them with the chemotherapeutic drug doxorubicin (DOXO) and the DO-24 monoclonal antibody (mAb) directed against the Met/Hepatocyte Growth Factor receptor (Met/HGFR), which is over-expressed on different types of carcinomas and thus represents a useful tumor target. The chemical-physical features of the nanoparticles were fully investigated and their interaction with cells expressing (GTL-16 gastric carcinoma line) or not expressing (NIH-3T3 fibroblasts) the Met/HGFR was analyzed. Functionalized nanoparticles specifically bound to and were internalized in cells expressing the receptor (GTL-16) but not in the ones that do not express it (NIH-3T3). Moreover they discharged DOXO in the targeted GTL-16 cells that reached the nucleus and displayed cytotoxicity as assessed in an MTT assay. Two different types of ternary nanoparticles were prepared, differing for the sequence of the functionalization steps (adsorption of DOXO first and then mAb or viceversa) and it was found that the ones in which mAb was adsorbed first were more efficient under all the examined aspects (binding, internalization, cytotoxicity), possibly because of a better mAb orientation on the nanoparticle surface. These multifunctional nanoparticles could thus be useful instruments for targeted local or systemic drug delivery, allowing to decrease the therapeutic dose of the drug and thus adverse side effects. Moreover, this work opens new perspectives in the use of nanocrystalline apatites as new platform for theranostic applications in nanomedicine.

1. Introduction

Current nanotechnologies are offering new opportunities in different fields, including medicine. In the field of oncology, nanoparticles (NPs) are promising tools as drug delivery vehicles and imaging probes for the unique properties linked to their size.[1-4] The dimension

(≤ 100 nm) allows their prolonged circulation in the blood stream escaping the capture from macrophages and the selective accumulation (passive targeting) within the tumor sites, via the so-called enhanced permeability and retention (EPR) effect.[1, 2] NPs have a high surface/volume ratio and surface bioreactivity, which makes them potential multifunctional platforms, since they can be coupled with different types of molecules, such as targeting moieties specifically recognizing tumor markers (active targeting), drugs and imaging probes. Both passive and active targeting drug nanocarriers should display improved anti-cancer activity, by increasing the concentration of drug in the primary and in the metastatic tumor, while significantly reducing non specific toxicity towards normal cells and thus the severe toxic side effects linked to chemotherapeutics.[3] NPs can respond to local stimuli *in vivo*, e.g. specific pH or temperatures[3, 5] and they can be produced with different types of materials, e.g. from inorganic compounds to organic or biological materials.[3, 6]

Nanocrystalline apatite (Ap) possesses ideal features of biocompatibility, because of its structural and chemical similarity with the mineral component of mammalian bones and dentin.[7] Traditionally, apatite based materials are used for bone repair applications due to their well known properties such as osteoinductivity and bioactivity.[6, 8] The recent advances in the structural characterization at the nanoscale level and in the colloidal stabilization of apatite nanocrystals have opened new perspectives in their use as drug carriers in nanomedicine.[9-11] In particular, they display several advantages in comparison with other nanomaterials most commonly used in this context, such as: i) favorable biodegradability and biocompatibility properties in general; ii) higher degradability and lower toxicity than silica, quantum dots, carbon nanotubes, or metallic magnetic particles; iii) higher stability than liposomes, allowing a more controlled and predictable drug delivery.[12] Indeed, in contrast to liposomes and other micelle-based carriers, which can undergo dissipation (which represents a clear obstacle upon injection into the bloodstream), apatite-based systems are negligibly

soluble in blood, which is by itself saturated with respect to apatite. Moreover, they generally show higher biocompatibility and pH-dependent dissolution compared to most of the polymers in use.[13] Apatites dissolve into their ionic constituents (Ca^{2+} and PO_4^{3-}), whose concentrations range from nano- to millimolar in cells and in the bloodstream, respectively.[14] Their dissolution avoids undesirable nanoparticle accumulation in cells and tissues, a drawback often encountered with other inorganic and metallic nano-systems.[15] On the other side, the rapid increase of intracellular Ca^{2+} above physiological concentrations can contribute to apoptosis, as suggested by few reports.[16] Generally, however, cells can counteract sudden rises of intracellular Ca^{2+} levels, by pumping ions in intracellular Ca^{2+} stores, such as mitochondria, endoplasmatic reticulum, or out of the cell. This discrepancy in the data could be ascribed to the particular cell types or, more probably, to the aggregated state of the apatite;[17] iv) nanocrystalline apatites can bind a wide variety of molecules, due to the presence of available surface ionic sites (i.e. $>Ca^{\delta+}$ and $>PO^{\delta-}$)[18] and in high amounts, due to the high surface/volume ratio.[19-21] Indeed in the recent years they have been coupled with (many) different types of molecules, namely for imaging (organic dyes and lanthanides), therapeutic delivery (oligonucleotides, chemotherapeutics, antibiotics, etc.) and targeting tumor cells (ligands for cell surface receptor, antibodies).[14, 22, 23] In this way, active targeting moieties as well as therapeutic agents can be incorporated into the nanoparticles to specifically enhance the effect of the active components.

Targeting exploits the presence of tumor specific or tumor associated markers, i.e. molecules preferentially expressed on tumor cells. Receptors for growth factors, such as folic acid,[24] transferrin[25] and tyrosine kinase receptors[26, 27] are often over-expressed on tumor cells and thus have been used as targets for the cognate ligands or antibodies. In most cases, targeted nanoparticle binding triggers its receptor-mediated endocytosis and thus internalization of coupled drug payload.[28, 29]

Met is the tyrosine kinase receptor of HGF and it has been shown to be involved in cancerogenesis and in the metastatic process, when it is activated in an uncontrolled way, promoting abnormal cell proliferation, migration, invasion, and angiogenesis.[30] Met, which can be aberrantly activated upon mutation, gene amplification and overexpression, is associated with the development of many types of cancers, mainly carcinomas and hematologic malignancies[30-32] and can be a marker of the metastatic progression.[33] The strong association between aberrant expression of Met and tumorigenesis provide a strong rationale for targeting this molecule in cancer treatment.[30, 34, 35] Different kinds of molecules have been developed, namely small-molecule inhibitors of the kinase activity and for this reason not strictly specific, since they can target also other tyrosine kinases, and more specific biological molecules designed on the basis of the structure of HGF or Met. Among these there are fragments of the ligand or of the receptor which interfere with receptor activation[36, 37] or neutralizing antibodies.[38] A scFv antibody has recently been used as targeting moiety on doxorubicin liposome carriers.[39]

Herein we report the development and properties of targeted delivery system based on apatite nanocrystals functionalized both with monoclonal antibodies (mAb) for targeting the Met receptor and with the chemotherapeutic drug doxorubicin (DOXO). Binary (Ap-mAb and Ap-DOXO) and ternary (Ap-mAb-DOXO and Ap-DOXO-mAb) nano-systems were produced and characterized. The interaction with the gastric carcinoma cell line GTL-16 and the *in vitro* anti-tumor cell activity of these nanocarriers were investigated.

2. Results and discussion

2.1 Characterization of apatite nanoparticles

Plate-shaped biomimetic apatite (Ap) nanocrystals were synthesized by a precipitation method.[40] The bulk Ca/P ratio (1.62) was slightly lower than the stoichiometric one (1.67),

and a limited amount of carbonate groups (about 2% wt), derived from the CO_2 dissolved in the preparation media was present (Table S1). Ap exhibited a high specific surface area (SSA), within the 150–170 m^2g^{-1} range. The X-ray powder diffraction pattern (XRPD) of apatite (Figure S1A) displayed the characteristic reflections of hydroxyapatite single phase (JCPDS 9-432). It exhibited broad diffraction peaks corresponding to a low degree of crystallinity and nano-sized crystal domains. The nanocrystals appeared elongated along the *c*-axis of the hexagonal structure. Their average crystal domain sizes were estimated using the Scherrer's formula. The average length, determined from the (002) peak at $2\theta = 25.9°$ was23 ± 4 nm, whereas the average width, derived from the (310) peak at $2\theta = 39.6°$ was 9 ± 3 nm (Table S1).TEM observations confirmed the nanosized dimensions of the apatite. In fact, the image (Figure S1B) reveals that they appeared as irregularly shaped plate-like particles whose lengths range between 35 and 45 nm. The FT-IR spectra (Figure S1C) assessed the presence of the typical absorption bands of apatite. The broadness of the IR bands supported the low crystallinity found out by XRPD. Detailed studies of the FT-IR bands of carbonate ν_3 (1350–1600 cm^{-1}) suggested a B-type carbonate substitution (i.e., carbonate replacing phosphate) in the apatite structure. Moreover, the low intensity of the band corresponding to the OH libration mode of apatite at 632 cm^{-1} indicated the poor hydroxylation feature typical of biomimetic apatite with regard to the stoichiometric hydroxyapatite. Dynamic light scattering (DLS) measurements showed that the size of the dispersed NPs showed an average size of 44 nm (Figure S1D), which is in good agreement with the values found by TEM observations. These characterizations indicate that the synthetic Ap developed in the current study displayed in an excellent way the chemical and morphological features of nanocrystalline apatites of biological origin, in particular those of bone origin. The much faster dissolution of Ap at pH 5.0 than at physiological pH (Figure S2) confirmed its potential use as pH dependent-nanocarrier.

2.2 Preparation and characterization of functionalized nanoparticles

Ap nanocarriers were functionalized with DOXO as chemotherapeutic agent and with the monoclonal antibody (mAb) DO-24, an IgG 2a/k mAb produced against the ectodomain of the human Met/HGF receptor and reacting with the receptor of different species[32, 41] as targeting moiety. Both binary (i.e. Ap NPs coupled with DOXO or with the mAb) and ternary (Ap-DOXO-mAb and Ap-mAb-DOXO) NPs were prepared. In the preparation of binary NPs the maximum amounts of DOXO and DO-24 mAb loaded on Ap nanocrystals were quantified to be 2.2 mg/m^2 (0.26 mg/mg) and 2.5 mg/m^2 (0.30 mg/mg), respectively. The amount of mAb adsorbed on Ap NPs is in good agreement with the value reported by Iafisco et al.[40]when human IgG were adsorbed onto the same nanocrystals. To prepare ternary NPs, two different combinations were used, i.e. DO-24 mAb coupling first and DOXO in the second step (hereafter Ap-mAb-DOXO), or viceversa first DOXO coupling and then DO-24 mAb (hereafter Ap-DOXO-mAb). In agreement with the work of Iafisco et al.[40] adsorption on Ap did not induce significant secondary structure modification of the mAb, which bound with the preferential end-on orientation, probably through their Fc domain because of the steric hindrance of their Fab domains. Indeed, to maximize the amount of adsorbed mAb in the more appropriate orientation for antigen recognition, saturating amount of mAb (an initial value higher than the maximum loading capacity) was used for the preparation of ternary NPs (2 mg mAb/5 mg Ap/1 mL). Not-saturating amount of DOXO (1 mg DOXO/5 mg Ap/1 mL) was used in order to have available space on Ap for mAb adsorption in the preparation of Ap-DOXO-mAb samples. The same DOXO amount was used also in the production of Ap-mAb-DOXO. In this way, the same amount of DOXO and mAb were found to be bound in both types of ternary NPs, irrespective of the coupling sequence (see also Figure 3, lanes 4 versus

lane 5) namely 1 mg of DOXO and 2 mg of mAb on 5 mg of Ap. This finding was confirmed also by the immuno-precipitation tests (see Figure 3, lanes 4 versus lane 5).

The effective binding of DOXO and DO-24 mAb on Ap NPs was verified by Raman spectroscopy (Figures 1A and 1B). The Raman spectra of the Ap-DOXO and Ap-mAb (**Figure 1**A) binary nano-assemblies displayed the typical apatite bands[42] (marked with an asterisk) as well as the peaks assignable to DOXO and mAb (Raman shifts in red and blue colors in Figure 1A, respectively). Namely, the most intense peaks at *ca.* 443, 1211 and 1244 cm^{-1} evidenced the DOXO fingerprint[43] whereas the band between 1250 and 1700 cm^{-1}involved the amide III and amide I groups of the mAb.[40] The Raman spectra of the ternary NPs prepared by the two approaches (**Figure 1**B) confirm the presence of both mAb and DOXO adsorbed on the Ap surface.

ζ-potential (**Figure 1**C) and DLS measurements (**Figure 1**D) were carried out to investigate the surface charge and the size distributions of the binary and ternary NPs. The mean ζ-potential of Ap at pH 7.4 is slightly positive (+1.9 mV) due to the balancing between of positive ($>Ca^{\delta+}$) and negative ($>PO^{\delta-}$) ionic surface groups. When Ap NPs were coupled with DOXO the ζ-potential increased to +29.3 mV. Protonated DOXO molecules form dimers in aqueous solutions being the anti-parallel the most stable configuration (with the $–NH_3^+$ groups in opposite directions).[44]Thus, after interaction of the dimer through part of its positive -NH_3^+ groups with the negative ($>PO^{\delta-}$) groups of the Ap surface, the resulting binary nano-assemblies display the NH_3^+ groups directed toward the surrounding solution. On the contrary, Ap functionalized with the DO-24 mAb showed a negative ζ-potential value (-17.9 mV) indicating a preferential affinity of the mAb through electrostatic interactions for the Ca^{2+} ions of Ap. Moreover, because of steric hindrance the mAb would preferentially bind through its Fc domain, exposing the Fab fragments. This hypothesis is in agreement with the theoretical work of Sidorov et al.[45]and it is well supported by the immunoprecipitation experiments (see

below). Different distributions of the ζ-potential were found for the ternary Ap-mAb-DOXO and Ap-DOXO-mAb NPs. The former exhibited a sharp distribution with the maximum centered at a slightly positive value (+1.4 mV), whereas Ap-DOXO-mAb showed a broad distribution (from -50 to +15 mV) with the maximum centered at -18.2 mV. The ζ-potential of Ap-mAb-DOXO is explained on the basis of the balance between mAb and DOXO adsorption (**Figure 2**, method 1). In the first step mAb adsorbs on Ap through its Fc fragment and display the Fab fragment towards the surrounding solution. In the second step, DOXO adsorbs on the remaining free adsorption sites of Ap nanocrystals, displaying positive $-NH_3^+$ residues toward the surrounding solution. On the contrary, the sequence DOXO first and then mAb could lead to different situations responsible of the broad distribution of ζ-potential values (**Figure 2**, method 2), i.e. mAb could be bound directly to Ap through its Fc fragment or to the adsorbed DOXO, either through its Fc or Fab fragments.

The mean hydrodynamic radius (R_h) measured by DLS for the Ap-mAb NPs was 61.4 nm while the mean R_h for the non-functionalized Ap was 44 nm. This finding agrees with an end-on configuration of mAb adsorbed on Ap (length around 12 nm[46]). The two ternary NPs showed different R_h values. The mean R_h of Ap-mAb-DOXO was 65.4 nm whereas that of Ap-DOXO-mAb was 50.4 nm. These findings support the fact that Ap-DOXO-mAb NPs can show different configurations including the mAb in the edge-on orientation, explaining why the R_h value is closer to that of non-functionalized Ap (44 nm, Figure S1D).

The stability of the binding moieties under physiological conditions was tested by incubating the ternary NPs at 37 °C for different times up to 3 days in a buffer at pH 7.4 (physiological conditions), or in a buffer at pH 5.0, mimicking the acidic environment typical of endosomes/lysosomes. At pH 7.4 no significant release of mAb and DOXO was detected, whereas about the 80% of the bound DOXO, as well as of the mAb, were released upon 3 days at pH 5.0 (data not shown). These values are in line with the data relative to the

dissolution of unfunctionalized NPs (Figure S2). The integrity of the two types of ternary NPs at pH 7.4 suggests that both can reach the target cells without losing the functional moieties.

When the immunocompetence of the different NPs was assayed, only those NPs carrying the mAb, but not the NPs functionalized with DOXO alone, were found to recognize the Met antigen solubilized from GTL-16 cells, which was visualized in western blots with the appropriate anti-Met DL-21 antibody (**Figure 3**, lanes 3-5) as a 145 kDa band, corresponding to the receptor β chain. In this analysis also the 170 kDa Met precursor was recognized. The specificity of the reaction was further confirmed when extracts from cells not expressing the Met antigen were reacted with the DO-24 mAb functionalized NPs. In this case the typical band corresponding to the Met antigen was not detected (Figure 3, lane 1). No difference was found in terms of amount of mAb adsorbed onto the two kinds of ternary NPs confirming a similar loading efficiency (Figure 3, IgG H chain in lanes 4, 5). However, for the same amount of DO-24 mAb adsorbed on the two types of ternary NPs, the ones where the mAb was adsorbed before the adsorption of DOXO were found to react with the Met antigen more efficiently than the ones where DOXO was adsorbed before the mAb (Figure 3, lane 5 versus lane 4). The greater functionality of Ap-mAb-DOXO relative to the other ternary NP could be expected on the basis of the adsorption model discussed above.

2.3 Cellular uptake of functionalized nanoparticles

The interaction of the different functionalized NPs with cells was evaluated by confocal microscopy. First the specificity of the binary DO-24 mAb-loaded Ap NPs was assessed upon incubation at 37°C for 3 h and staining with FITC-labelled anti-mouse Ig. These NPs were found to be detectable only in GTL-16 cells, which overexpress the Met receptor (**Figure 4**, top row), but not in the case of NIH-3T3 fibroblasts, which do not express the receptor (Figure 4, medium row). They were mainly localized at the surface and intracellularly in

vesicles, after being internalized within the endosomal/lysosomal compartment, as shown by their co-localization with Lysotracker®-positive vesicles (Figure 4, bottom row),

Nanoparticles loaded with an antibody of IgG2a/k isotype directed against an unrelated antigen, which was used as control, did not bind (not shown).

After validating the mAb-dependent specificity of the functionalized Ap NPs, the two ternary NPs were tested for their interaction with GTL-16 cells. **Figures 5**A and 5B show the confocal microscopy images of the ternary complexes Ap-mAb-DOXO and Ap-DOXO-mAb after incubation for 3 hours at 37°C with GTL-16 cells, respectively. Comparing confocal images 5A and 5B, it can be clearly distinguished, in both cases, green fluorescence revealing mAb-loaded NPs at the cell surface or in its proximity and red fluorescence corresponding to DOXO inside the cells. However, the green color is much stronger for the Ap-mAb-DOXO (Figure 5A) than for the Ap-DOXO-mAb (Figure 5B). Additionally, while DOXO is mainly localized in the nucleus when using Ap-mAb-DOXO assemblies, it is equally distributed within the whole cells when the other ternaries are employed. Therefore, the Ap-mAb-DOXO system was found to bind at the cell surface with higher efficiency and moreover to release DOXO in the nucleus more efficiently (Figure 5A).

In neither case mAb-related signals were detected within the nucleus, thus strongly suggesting that also NPs to which they are bound were not translocated there. Indeed it is acknowledged that nuclear translocation is strictly controlled and meets many requirements[28, 47] and in other drug delivery systems based on NPs, the latter were never detected in this cellular compartment.[27] By contrast, as already described herein in the case of binary nanoparticles, ternary nanoparticles were detected either at the cell surface or intracellularly in endocytic vesicles in close proximity to the cell surface.

On the basis of the above data, in conjunction with data obtained in the experiments performed for different incubation time (Figure S3) we can propose the following mechanism

regulating cell internalization of the nanoparticle components. After mAb-mediated binding to the cell surface receptor, which is a passive step occurring also at 4 °C, NPs are endocytosed by an active process occurring at 37 °C.[48] Once inside the cell, DOXO is released from the NPs and translocated to the nucleus possibly through the formation of a DOXO–proteasome complex.[49, 50] Indeed, even in the case of DOXO covalently bound to other types of NPs, DOXO is released and no trace of the carrier is detected in the nucleus.[27] This is an active and selective process, occurring only at 37°C, which is essential for the drug to reach its target organelle. On the other side, the observation that ternary NPs could be detected only at the cell membrane or in the internalized vesicles near the cell membrane may also suggest that, while DOXO is quickly discharged and translocated to the nucleus, NPs still loaded with the antibody and bound to the receptor could be recycled to the cell membrane. Indeed it is accepted that endocytosed tyrosine kinase receptors may recycle to the plasma membrane.[51, 52] Moreover, it is also expected that a certain amount of mAb-loaded NPs might be degraded within the endosome-lysosome compartment.[48, 51, 53]

Internalization efficiency correlates with the binding efficiency, which then affects also relocalization of DOXO to nucleus. Different factors could be implied in the more efficient behavior of Ap-mAb-DOXO relative to Ap-DOXO-mAb NPs. The difference in size between the mAb molecules –about 150000 Daltons- and DOXO –544 Daltons- could affect the binding of the mAb, due to steric hindrance, if this was coupled in the second step. As already discussed, steric hindrance would promote a more functional spatial orientation of the mAb, with the Fab better exposed allowing an easier recognition of the receptor. In Ap-mAb-DOXO there might be a higher propensity of DOXO to be discharged, since possibly present in a more external position on the nanoparticle. Moreover, the ζ-potential of the two types of the ternaries conjugates, which indeed is dictated by the sequence of functionalization steps and was found to be significantly different, could play an important effect. Indeed, the Ap-

DOXO-mAb system shows a broad range of ζ-potential values centered at -18.4 mV; thus, only the complexes with positive values could efficiently interact with the negatively charged cell surface, if electrostatic interactions are considered. By contrast, the ζ-potential distribution measured for the Ap-mAb-DOXO assemblies was centered at positive values (+1.4 mV) thus favoring the interaction of most of the conjugates with the negatively charged cell surface. In both cases, however, interaction of the ternary NPs will be controlled by the specific recognition exerted by the mAb.

2.4 *In vitro* cytotoxicity of functionalized nanoparticles

The anti-proliferative activities of the different NPs loaded with DOXO, as well as of soluble free DOXO, were tested on the GTL-16 carcinoma cell line using a standard tetrazolium assay (MTT) (**Figure 6**). Figure 6A represents the effective toxicity as a function of DOXO equivalent concentrations after incubation for three days. At all concentrations tested, ternary Ap-mAb-DOXO NPs displayed a toxic activity similar to that of Ap-DOXO, reducing cell survival to about 40-30% relative to control untreated cells. The other ternary NPs (Ap-DOXO-mAb) were not as effective, although they were loaded with equivalent amounts of both doxorubicin and monoclonal antibodies. This finding could be expected on the basis of their lower cellular binding and lower ability to drive DOXO nuclear accumulation. Nanoparticles functionalized only with the antibody, as well as unfunctionalized NPs, did not display significant toxicity, reducing cell viability to about only 85-90% (Figure 6B), in line with what extensively reported in the literature, showing that nanosized apatites are not toxic, even when used at concentrations reaching 50-200 μg/ml.[16, 23, 54] Ap-DOXO and Ap-mAb-DOXO were less cytotoxic than free DOXO under all cell culture conditions, probably because of their slower rate of internalization and of the longer time required for their nuclear accumulation relative to free DOXO (data not shown). Similar findings were reported also for

other DOXO-loaded NPs prepared with different carriers by other groups[27, 55] and do not represent a drawback of these compounds. Indeed this can be viewed as a decreased aspecific cytotoxic potential and this reduced activity is largely compensated by their ability to circulate in the blood stream for longer periods of time, allowing them to passively reach the tumor target through the EPR effect.[1] Active targeting, especially in vivo, should definitively direct the ligand functionalized NPs to the tumor cells overexpressing the cognate receptor.

3. Conclusions

Although there have been undeniable advances in the development of therapies for various cancers in recent years, cancer remains a major health challenge, being still the second cause of mortality in western countries. Nanotechnologies offer new therapeutic opportunities, besides the more traditional treatments such as surgery, radiotherapy and chemotherapy, their major advantage being the possibility to target specifically tumor cells, reducing the amount of the drug and by consequence reducing also the severe side effects generally associated with it. In this context we have developed and characterized apatite nanoparticles loaded with doxorubicin and a monoclonal antibody recognizing the Met receptor as targeting moiety. These multifunctional NPs interacted specifically with their target cells, were uptaken and able to deliver them DOXO, which was then internalized within the nucleus and displayed its cytotoxic activity on the tumor cell line.

Doxorubicin is one of the most popular anti-cancer drug, but its clinical application is limited by its severe side effects, namely cardiotoxicity.[35, 50, 56] Its use is now being re-evaluated in the context of the emerging drug delivery nanotechnologies, both at experimental level[27, 57]and in clinical applications.[58, 59]

Herein we have used apatite as nanocarrier for its high biocompatibility, biodegradability and responsiveness to pH changes. Apatite is a natural structural component of the body and is

quite stable at the neutral physiological pH, such as in the blood stream, but it dissolve and can release the adsorbed drug at pH around 5. This pH is found only in peculiar situations such as in the endosome-lysosome compartment, involved after receptor-mediated nanoparticle uptake. A slightly less acidic pH is present also in the peritumoral sites. We found that both DOXO loaded NPs, either binary or ternary, displayed a lower toxicity than free DOXO. *In vivo* this could be an advantage since NPs, which are endowed of longer half-life in the blood circulation, can accumulate at the tumor site through the EPR effect and active targeting[1, 2] in the case of ternary NPs thus releasing there their payload drug. At the same time, healthy cells should be spared. Finally, the fact that apatite dissolves releasing Ca^{2+} and PO_4^{3-}, which can be easily recycled, avoids the problem of eliminating possibly toxic nanocarrier byproducts, as in the case of other compounds (silver, silica, gold, copper, etc.).[60]

Targeted NPs were able to discriminate between cells expressing or not the relevant tumor associated marker Met. Moreover *in vivo* cells will compete for binding the mAb-loaded NPs and the ones expressing higher levels of receptor will be able to recruit them at their surface more efficiently. As in the case of other tyrosine kinase receptors,[61, 62] also Met, when is overexpressed, is directly involved in the processes of tumorigenesis and metastasis. These are dependent on the biologic cellular responses the receptor mediates, namely cell proliferation and migration, which, when combined, result in the so-called invasive growth.[63] Met is found overexpressed in many types of cancer and can be considered a marker of the metastatic progression.[30] It is largely acknowledged that the major problem in cancer is not the primary tumors, but the metastasis, where also neoangiogenesis is involved. Since Met is expressed also on endothelium, NPs targeting Met should be able to attack tumors also on this side. Due to the central role of Met in tumorigenesis, many therapeutic molecules have been developed, but only few with strict specificity, based on fragments of the ligand or of the

receptor or antibodies directed against them.[37, 38] In particular, recently an scFv antibody was used as targeting moiety on pegylated liposomes.[39] These nanocarriers delivered DOXO efficiently, increased drug accumulation and displayed anti-tumor activity *in vivo*. Moreover they allowed imaging through quantum dots.[39] In this work we used full-size antibodies as Met targeting moiety and we found that the sequence of the two adsorption steps, relative to DOXO and the antibody, impacted on the biologic activity of the NPs. To obtain NPs endowed of higher binding and up-taking activity, which then correlates with the cytotoxic activity, the antibody must be adsorbed before DOXO.

Different factors could be implied in the more efficient behavior of Ap-mAb-DOXO relative to Ap-DOXO-mAb NPs: a more functional exposition of mAbs at the nanoparticle surface, a higher propensity of DOXO to be discharged, since possibly present in a more external position on the nanoparticle and finally the nanoparticle ζ-potential, which is slightly positive and dictated by the sequence of the functionalization steps. Indeed, in the case of Ap-DOXO-mAb complexes the negative ζ-potentialcould disfavor the interaction with the negatively charged cell surface. This should be taken into account when planning NP functionalization. The data obtained here are thus the basis for future *in vivo* experiments and open new perspectives for future studies in the use of nanocrystalline apatite as new tool for diagnostic as well therapeutic applications in nanomedicine.

4. Experimental section

Materials: Common high-purity chemical reagents, as well as doxorubicin hydroxchloride (DOXO) (98-102% HPLC) suitable for fluorescence, 3-(4,5-Dimethylthiazol-2-yl)-2,5-diphenyltetrazolium bromide) (MTT), Triton-X100, Tetramethylrhodamine isothiocyanate (TRITC)-phalloidin were supplied by Sigma Aldrich (St. Louis, MO, USA). Polyvinylidene Fluoride membranes, horseradish peroxidase-conjugated affinity-purified rabbit anti-mouse

IgG antibodies (RaHIgG/PO) and Enhanced Chemiluminescence (ECL) kit were from Amersham (GE Healthcare Europe GmbH, Milano, Italy); fluorescein isothiocyanate-labeled secondary antibodies were purchased from Abcam (Cambridge, UK); TO-PRO-3 and Lysotracker® DND-99.from Life Technologies (Monza MB, Italy). All reagents for tissue culture (Dulbecco's modified Eagle medium, Fetal Bovine Serum, penicillin and streptomycin) were from Lonza (Basel, CH). Ultrapure water (0.22 mS, 25 °C) was used in all experiments

Synthesis of nanocrystalline apatites: Apatite (Ap) nanocrystals were synthesized according to the method reported by Liou et al.[64] Briefly, the nanocrystals were precipitated from a suspension of $Ca(CH_3COO)_2$ (0.35 M) by the slow addition (1 drop s^{-1}) of an aqueous solution of H_3PO_4 (0.21 M), keeping the pH at a constant value of 10 by the addition of a $(NH_4)OH$ solution. The reaction mixture was kept under stirring at room temperature for 24 hours, then stirring was suspended and the mixture was left standing for 2 hours to allow deposition of the inorganic phase. This latter was isolated by centrifugation of the reaction mixture, repeatedly washed with water, and freeze-dried at -60 °C under vacuum (3 mbar) overnight. Apatite granular fractions having dimensions <38 μm (400 mesh) was selected for the study by sieving the powder.

Functionalization of nanoparticles: Ap was functionalized with DOXO as well as with the monoclonal antibody DO-24, an IgG 2a/k monoclonal antibody (mAb), produced against the ectodomain of the human Met/HGF receptor.[32, 41] Experiments were performed to assess the maximum amount of DOXO and mAb loading on the nanoparticles by mixing 5 mg of Ap with 1 mL of different concentration (ranging from 0.1 to 5 mg/mL) of DOXO dissolved in water or purified mAb dissolved in Hepes buffered saline solution (0.01 M Hepes, 0.15 M NaCl) in a 2 mL conical polyethylene Eppendorf tube. Mixtures were maintained in a bascule bath at 37 °C for 24 h. In all further experiments (to prepare binary as well as ternary

nanoparticles), a solution of 2 mg/ml of antibody and 1 mg/ml of DOXO were then incubated with 5 mg of apatite nanoparticles. DOXO and mAb content were assessed by UV-Vis spectroscopy (λ = 495 and 280 nm, ε = 10650 and 64000 M^{-1} cm^{-1} respectively) indicative of the concentrations of the two molecules by comparison to standard curves. The amount of adsorbed molecules was calculated from the differences between the concentrations of the molecules solutions before and after the adsorption on Ap (the so-called supernatant). The solid component was washed twice with ultrapure water, recovered by centrifuging at 10000 rpm (12700 g) for 3 min on a micro Centrifugette 4214 and then freeze-dried at -60 °C under vacuum (3 mbar) overnight.

In case of Ap conjugated with both moieties (DOXO and mAb) (the so-called ternary nanoparticles), the same protocols were sequentially applied, each one followed by extensive washings (i.e. DO-24 mAb coupling first and DOXO coupling in the second step, or viceversa first DOXO coupling and then DO-24 mAb).

Characterization of the functionalized nanoparticles: Raman spectra of the nano assemblies were collected with a 800 nm focal length LabRam HR spectrograph (from Jobin-Yvon, Horiba, Japan) using diffraction gratings of 600 lines/mm. The entrance slits were adjusted to 200 μm. The excitation laser beam (diode emitting at 785 nm) was focused through a 50x long-working distance objective (0.5 NA) into a 2 μm spot at surface of the powdered sample. A Peltier-cooled charge-couple device (CCD) (1064 x256 pixels) was used as detector. Raman spectra are the results of the signal averaging of at least three spectra with a spectral resolution better than 3 cm^{-1}. The Raman intensity units are counts per seconds (c.p.s.).

The surface charge of the functionalized nanoparticless was quantified by laser Doppler velocimetry as electrophoretic mobility (or ζ-potential) with a Zetasizer Nano ZS (Malvern Ltd., UK). Disposable cuvettes (DTS1061, Malvern Ltd., UK) were used as electrophoretic

cell. The particles were suspended in ultrapure water. Each measurement consisted on three repetitions of ten runs (3 seconds each). Four measurements were collected for each sample.

Size distributions of the nanoparticles and the functionalized nanoparticles were measured by Dynamic Light Scattering (DLS) with a Zetasizer Nano ZS (Malvern Ltd., UK). Low-volume quartz cuvettes (105.251-QS, Hellma, Germany) were used. The particles were suspended in ultrapure water. Ten runs of 30 seconds each were performed in each measurement. Four measurements were carried out for each sample and the mean value is shown as result as the percentage of number of particles.

The release of DOXO and mAb from ternary nanoparticles was assessed by incubating 5 mg of functionalized Ap nanoparticles in 1 ml of 0.1 M citrate buffer pH 5.0, or in PBS at pH 7.4 as control, at 37°C in continuous mixing and measuring the concentration by UV-Vis spectroscopy, as already described, of the supernants at different time points up to 3 days and referring the released amount as percentage of the amount that was adsorbed initially.

The immunocompetence of the mAbs coupled on nanoparticles was assayed by incubating them with clarified detergent extracts prepared from GTL-16 cells and NIH-3T3 as negative control in DIM buffer (50 mM Pipes pH 7.4, 300 mM saccharose, 100 mMNaCl, 5 mM EGTA, 5 mM $MgCl_2$ and 100 µM $ZnCl_2$), 1% Triton X-100, 1 mM TRIS HCl pH 8.8, and a cocktail of protease inhibitors), as described[65] at 4 °C for 2 h. Nanoparticles were then washed, proteins solubilized in Laemmly buffer, heated at 95 °C for 5 min, separated in 10% SDS-polyacrylamide gel electrophoresis, transferred on Polyvinylidene Fluoride membranes for Western blot and decorated with anti-Met DL-21 monoclonal antibody,[32] followed by horseradish peroxidase-conjugated affinity-purified rabbit anti-mouse IgG antibodies (RaHIgG/PO, 1:2000), reacted with enhanced chemiluminescence (ECL kit) and analyzed in a Versadoc instrument (Biorad, USA).

Cell cultures: The GTL-16 cells, a poorly differentiated human gastric carcinoma derived cell line and the NIH 3T3 murine fibroblasts (ATCC, CRL-1658^{TM}) were maintained in Dulbecco's modified Eagle's medium (DMEM), supplemented with 10% fetal calf serum (FCS), 50 U/ml penicillin, and 50 µg streptomycin. Cells were transplanted twice a week, when they were at 90-95% confluence, at 1/3-1/4 (GTL-16 cells) and 1/10 (NIH-3T3).

Cellular uptake: Cells (22 x 10^3 GTL-16 or 7.5 x 10^3 NIH-3T3/well) were seeded on glass coverslips in 24-well plates and after 24 h free DOXO or presaturated (in 0.4% BSA for 2 h at 37 °C) nanoparticle suspensions were added. After incubation at 37 °C for different periods of time (from 5 min to 3 h), coverslips were washed twice with fresh Phosphate Buffered Saline (PBS), pH 7.2, fixed with paraformaldehyde (2 wt% in PBS), permeabilized with 0.1% Triton-X100 in PBS, containing 2% bovine serum albumin and stained. In particular cytoskeletal actin microfilaments were stained with TRITC-phalloidin (1/100, Sigma-Aldrich excitation at 543 nm; emission at 560-620 nm), mAbs with FITC-labelled rabbit-anti-mouse IgG (1/500, Abcam excitation at 488 nm; emission at 500-535 nm), nuclei with TO-PRO-3 (1/100, Life Technologies; excitation at 633 nm; emission at 650-750 nm), endosomes/lysosomes with Lysotracker® DND-99.(1/100, Life Technologies, excitation at 577 nm; emission at 590 nm). DOXO was detected after excitation at 476 nm and emission at 575-630 nm. Fluorescence was detected using a Leica TCS SP2 AOBS Spectral Confocal Scanner microscope. Images were taken at 630x magnification. ImageJ® software was used for further analysis.

Cytotoxicity assay: GTL-16 cells were incubated (10 x 10^3/0.4 cm^2microwell) for 24 hours; then different concentrations of soluble DOXO, or functionalized nanoparticles were added in 100 µl. Equimolar amounts of DOXO, either soluble or coupled to nanoparticles as well as of unfunctionalized nanoparticles, were used. After 2-3 days incubation, cells viability was evaluated by the 3-(4,5-Dimethylthiazol-2-yl)-2,5-diphenyltetrazolium bromide) (MTT)

colorimetric assay. Briefly, 20 µl of MTT solution (5 mg ml^{-1} in a PBS solution) were added to each well. The plate was then incubated at 37 ºC for 3 hours and then supernatants were carefully aspirated. Afterwards, 125 µl of isopropanol 0.2 N HCl was added to dissolve formazan crystals. 100 µl were then removed carefully and the optical density was measured in a multiwell reader (2030 Multilabel Reader Victor TM X4, PerkinElmer) at 570 nm. Viability of parallel cultures of untreated cells was taken as 100% viability and values obtained from cells undergoing the different treatments were referred to this value. Experiments were performed 4 times using 3 replicates for each sample.

*Statistical analysis:*The experiments were performed in triplicates. Data are expressed as mean ± error standard. Statistical analyses were performed using independent t-tests for two groups comparisons and a one-way analysis of variance (ANOVA), after checking homogeneity of variance using Levene'stes, in case of multiple comparisons. ANOVA was followed by post-doc Scheffè's test. Differences at $p<0.05$ were considered to be statistically significant.

Acknowledgment

The Authors gratefully thank Dr. Donato Colangelo and Dr. Ezio Perucco for their help in the experiments of cytotoxicity and confocal microscopy. This work was supported by the Spanish MINECO through projects (Spanish-Italian Integrated Action ref. IT2009-00028, Crysfunbioref. MAT2011-28543 and "Factoría de Cristalización" of Consolider-Ingenio 2010), the Junta de Andalucía (Excellence project ref. RMN5384), project 30258/DB2001 (Ricerca Finalizzata 2009 from Regione Piemonte, Italy) and local funds from Università del Piemonte Orientale "A. Avogadro". MI and AT acknowledge the PNR-CNR Aging Program 2012-2014 and the Flagship Project NanoMAX (PNR-CNR 2011-2013). JMD acknowledges

Spanish CSIC for his postdoctoral JAE-DOC contract within the program “Junta para la Ampliación de Estudios” cofinanced by the European Social Fund (ESF).

[1] A. A. Manzoor, L. H. Lindner, C. D. Landon, J.-Y. Park, A. J. Simnick, M. R. Dreher, S. Das, G. Hanna, W. Park, A. Chilkoti, G. A. Koning, T. L. M. ten Hagen, D. Needham, M. W. Dewhirst, *Cancer Res.* **2012**, DOI 10.1158/0008-5472.can-12-1683.
[2] S. Pietronave, M. Iafisco, D. Locarno, L. Rimondini, M. Prat, *J. Appl.Biomater. Biomech* .**2009,** *7*, 77-89.
[3] T. L. Doane, C. Burda, *Chem. Soc. Rev.* **2012,** *41*, 2885-2911.
[4] X. Duan, Y. Li,*Small* **2012**, n/a-n/a. DOI 10.1002/smll.201201390.
[5] J. Zhu, L. Liao, X. Bian, J. Kong, P. Yang, B. Liu, *Small* **2012,** *8*, 2715-2720.
[6] S. Bose, S. Tarafder, *Acta Biomater.* **2012,** *8*, 1401-1421.
[7] N. Roveri, B. Palazzo, M. Iafisco, *Expert Opin.Drug Deliv.* **2008,** *5*, 861-77.
[8] M. Vallet-Regí, E. Ruiz-Hernández, *Adv. Mat.* **2011,** *23*, 5177-5218.
[9] A. Tabaković, M. Kester, J. H. Adair, *Wiley Interdiscip. Rev. Nanomed. Nanobiotechnol.* **2012,** *4*, 96-112.
[10] J. H. Adair, M. P. Parette, E. I. Altınoğlu, M. Kester, ACS Nano 2010, 4, 4967-4970.
[11] E. I. Altınoğlu, T. J. Russin, J. M. Kaiser, B. M. Barth, P. C. Eklund, M. Kester, J. H. Adair, *ACS Nano* **2008,** *2*, 2075-2084.
[12] V. Uskokovic, D. P. Uskokovic, *J. Biomed. Mater. Res. B Appl. Biomater.***2011,** *96*, 152-91.
[13] A. H. Faraji, P. Wipf, *Bioorgan. Med. Chem.* **2009,** *17*, 2950-2962.
[14] T. T. Morgan, H. S. Muddana, E. I. Altinoglu, S. M. Rouse, A. Tabakovic, T. Tabouillot, T. J. Russin, S. S. Shanmugavelandy, P. J. Butler, P.C. Eklund, J. K. Yun, M. Kester, J. H. Adair, *Nano Lett.* **2008,** *8*, 4108-4115.
[15] L. Lacerda, A. Bianco, M. Prato, K. Kostarelos, *Adv. Drug. Deliver. Rev.* **2006,** *58*, 1460-1470.
[16] M. Motskin, D. M. Wright, K. Muller, N. Kyle, T. G. Gard, A. E. Porter, J.N. Skepper, *Biomaterials* **2009,** *30*, 3307-3317.
[17] S. Neumann, A. Kovtun, I. D. Dietzel, M. Epple, R. Heumann, *Biomaterials* **2009,** *30*, 6794-6802.
[18] T. Boix, J. Gomez-Morales, J. Torrent-Burgues, A. Monfort, P. Puigdomenech, R. Rodriguez-Clemente, *J. Inorg.Biochem.***2005,** *99*, 1043-50.
[19] M. Iafisco, B. Palazzo, G. Martra, N. Margiotta, S. Piccinonna, G. Natile, V. Gandin,C. Marzano,N. Roveri, *Nanoscale* **2012,** *4*, 206-217.
[20] B. Palazzo, M. Iafisco, M. Laforgia, N. Margiotta, G. Natile, C. L. Bianchi, D. Walsh, S. Mann, N. Roveri, *Adv. Funct. Mater.* **2007,** *17*, 2180-2188.
[21] M. Iafisco, B. Palazzo, M. Marchetti, N. Margiotta, R. Ostuni, G. Natile, M. Morpurgo, V. Gandin, C. Marzano, N. Roveri, *J. Mater. Chem.* **2009,** *19*, 8385-8392.
[22] D. Kozlova, S. Chernousova, T. Knuschke, J. Buer, A. M. Westendorf, M. Epple, *J. Mater. Chem.* **2012,** *22*, 396-404.
[23] A. Al-Kattan, S. Girod-Fullana, C. Charvillat, H. Ternet-Fontebasso, P. Dufour, J. Dexpert-Ghys, V. Santran, J. Bordre, B. Pipy, J. Bernad, C. Drouet, *Int. J. Pharm.* **2012,** *423*, 26-36.
[24] N. V. Nukolova, H. S. Oberoi, S. M. Cohen, A. V. Kabanov, T. K. Bronich, *Biomaterials* **2011,** *32*, 5417-5426.

[25] B. M. Barth, R. Sharma, E. I. Altınoğlu, T. T. Morgan, S. S: Shanmugavelandy, J. M. Kaiser, C. McGovern, G. L. Matters, J. P. Smith, M. Kester, J. H. Adair, *ACS Nano* **2010,** *4*, 1279-1287.
[26] M. M. Cardoso, I. N. Peca, A C. A. Roque, *Curr. Med. Chem.* **2012,** *19*, 3103-3127.
[27] M. Shi, K. Ho, A. Keating, M. S. Shoichet, *Adv. Funct. Mater.* **2009,** *19*, 1689-1696.
[28] L. Rajendran, H.-J. Knolker, K. Simons, *Nat. Rev. Drug Discov.***2010,** *9*, 29-42.
[29] G. Sahay, D. Y. Alakhova, A. V. Kabanov, *J. Control. Rel.* **2010,** *145*, 182-195.
[30] E. Gherardi, W. Birchmeier, C. Birchmeier, G. V. Woude, *Nat.Rev. Cancer* **2012,** *12*, 89-103.
[31] D. Capello,G. Gaidano, M. Gallicchio, A. Gloghini, E. Medico, D. Vivenza, Buonaiuto, L. Fassone, G. C. Avanzi, G. Saglio, M. Prat, A. Carbone, *Leukemia* **2000,** *14*, 285-291.
[32] M. Prat, R. P. Narsimhan, T. Crepaldi, M. R. Nicotra, P. G. Natali, P.M. Comoglio, *Int. J. Cancer* **1991,** *49*, 323-328.
[33] G. Cortesina, T. Martone, E. Galeazzi, M. Olivero, A. De Stefani, M. Bussi, G. Valente, P. M. Comoglio, M. F. Di Renzo, *Int. J. Cancer* **2000,** *89*, 286-292.
[34] J. R. Sierra, M.-S. Tsao, *Ther. Adv. Med. Oncol* **2011,** *3*, S21-S35.
[35] P. M. Comoglio, S. Giordano, L. Trusolino, *Nat. Rev. Drug Discov.* **2008,** *7*, 504-516.
[36] A. R. Cantelmo, R. Cammarota, D. M. Noonan, C. Focaccetti, P. M. Comoglio, M. Prat, A. Albini, *Oncogene* **2010,** *29*, 5286-5298.
[37] P. Michieli, M. Mazzone, C. Basilico, S. Cavassa, A. Sottile, L. Naldini, P. M. Comoglio, *Cancer Cell* **2004,** *6*, 61-73.
[38] E. Vigna, G. Pacchiana, M. Mazzone, C. Chiriaco, L. Fontani,C. Basilico, S. Pennacchietti, P. M. Comoglio, *Cancer Res.* **2008,** *68*, 9176-9183.
[39] R.-M. Lu, Y.-L. Chang, M.-S. Chen, H.-C. Wu, *Biomaterials* **2011,** *32*, 3265-3274.
[40] M. Iafisco, E. Varoni, M. Di Foggia, S. Pietronave, M. Fini, N. Roveri, L. Rimondini, M. Prat, *Colloid Surface B* **2012,** *90*, 1-7.
[41] M. Prat, T. Crepaldi, S. Pennacchietti, F. Bussolino, P. M. Comoglio, *J. Cell. Sci.* **1998,** *111*, 237-247.
[42] J. M. Delgado-López, M. Iafisco, I. Rodríguez, A. Tampieri, M. Prat, J. Gómez-Morales, *Acta Biomater.* **2012,** *8*, 3491-3499.
[43] G. Das, A. Nicastri, M. L Coluccio, F. Gentile, P. Candeloro, G. Cojoc, C. Liberale, F. De Angelis, E. Di Fabrizio, *Microsc. Res. Techniq.* **2010,** *73*, 991-995.
[44] P. Agrawal, S. K. Barthwal, R. Barthwal, *Eur. J. Med. Chem.***2009,** *44*, 1437-1451.
[45] I. A. Sidorov, P. Prabakaran, D. S. Dimitrov, *J. Comput. Theor. Nanosci.* **2007,** *4*, 1103-1107.
[46] J. S. Bee, D. Chiu, S.Sawicki, J. L. Stevenson, K. Chatterjee, E. Freund, J. F. Carpenter, T. W. Randolph, *J. Pharm. Sci.* **2009,** *98*, 3218-3238.
[47] J. G. Turner, J. Dawson, D. M. Sullivan, *Biochem. Pharmacol.* **2012,** *83*, 1021-1032.
[48] A. Petrelli, G. F. Gilestro, S. Lanzardo, P. M. Comoglio, N. Migone, S. Giordano, *Nature* **2002,** *416*, 187-190.
[49] K.-i. Kiyomiya, S. Matsuo, M. Kurebe, *Cancer Res.* **2001,** *61*, 2467-2471.
[50] G. Minotti, P. Menna, E. Salvatorelli, G. Cairo, L. Gianni, *Pharmacol. Rev.* **2004,** *56*, 185-229.
[51] M. J. Clague,*Sci. Signal.* **2011,** *4*, pe40.
[52] H. M. Jopling, G. J. Howell, N. Gamper, S. Ponnambalam, *Biochem. Bioph. Res. Co.* **2011,** *410*, 170-176.
[53] M. Gonzalez-Gaitan, *Dev. Cell* **2008,** *15*, 172-174.

[54] J. Scheel, S. Weimans, A. Thiemann, E. Heisler, M. Hermann, *Toxicol. In Vitro* **2009,** *23*, 531-538.
[55] S. S. Padhye, S. Guin, H.-P. Yao, Y.-Q. Zhou, R. Zhang, M.-H. Wang, *Mol. Pharmaceut.* **2011,** *8*, 2310-2319.
[56] M. Volkova, R. Russell, *Curr. Card. Rev.* **2011,** *7*, 214-20.
[57] Y.-J. Lu, K.-C. Wei, C.-C. M. Ma, S.-Y. Yang, J.-P. Chen, *Colloid Surface B* **2012,** *89*, 1-9.
[58] A. Gabizon, H. Shmeeda, Y. Barenholz, *Clin. Pharmacokinet.* **2003,** *42*, 419-436.
[59] M. E. R. O'Brien, N.Wigler, M. Inbar, R. Rosso, E. Grischke, A. Santoro, R. Catane, D. G. Kieback, P. Tomczak, S. P. Ackland, F. Orlandi, L. Mellars, L. Alland, C. Tendler, *Ann. Oncol.* **2004,** *15*, 440-449.
[60] S. K Misra, A Dybowska, D Berhanu, S. N. Luoma, E. Valsami-Jones, *Sci. Total Environ.* **2012,** *438*, 225-232.
[61] D. J. Slamon, G. M. Clark, S. G. Wong, W. J. Levin, A. Ullrich, W. L. McGuire, *Science* **1987,** *235*, 177-182.
[62] T. A. Libermann, H. R. Nusbaum, N. Razon, R. Kris, I. Lax, H. Soreq, N. Whittle, M. D. Waterfield, A. Ullrich, J. Schlessinger, *Nature* **1985,** *313*, 144-147.
[63] C. Boccaccio, P. M. Comoglio, *Nat.Rev. Cancer* **2006,** *6*, 637-645.
[64] S.-C. Liou, S.-Y. Chen, H.-Y. Lee, J.-S. Bow, *Biomaterials* **2004,** *25*, 189-196.
[65] C. Bardelli, M. Sala, U. Cavallazzi, M. Prat, *Biochem. Bioph. Res. Co.* **2005,** *334*, 1172-1179.

Received: ((will be filled in by the editorial staff))
Revised: ((will be filled in by the editorial staff))
Published online on ((will be filled in by the editorial staff))

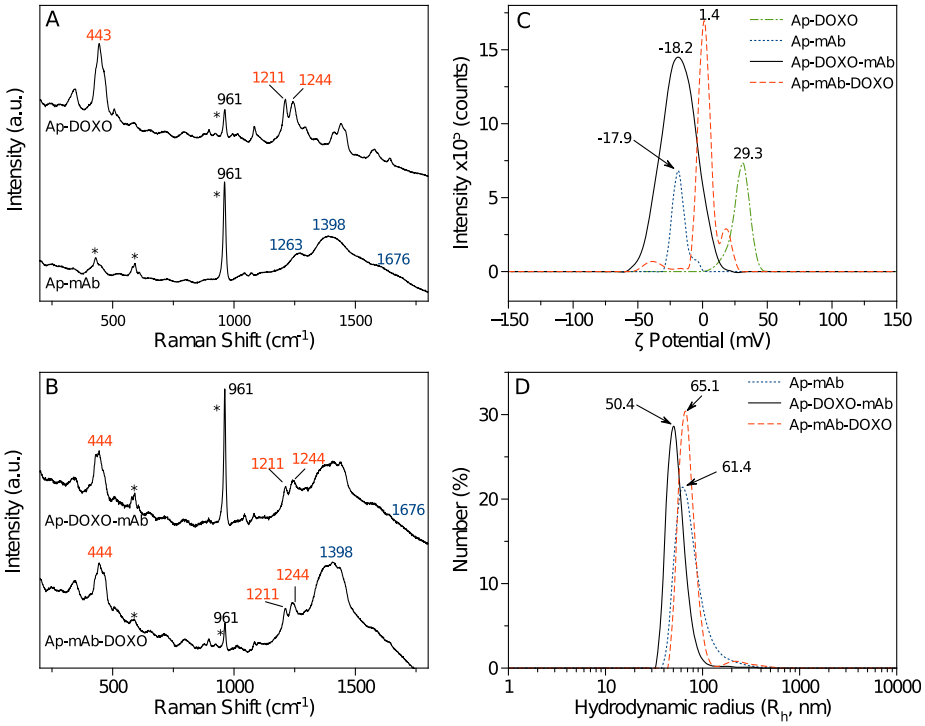

Figure 1. Raman spectra of the Ap-DOXO and Ap-mAb binary nanoparticles (A) and of Ap-mAb-DOXO and Ap-DOXO-mAb ternary nanoparticles (B). Asterisks indicate the Raman peaks of nanoapatite. ζ-potentials (C) and size distributions (D) of the binary and ternary nanoparticles. In Raman spectra (A and B), red-colored peaks belong to adsorbed DOXO molecules whereas blue-colored peaks are due to adsorbed mAb.

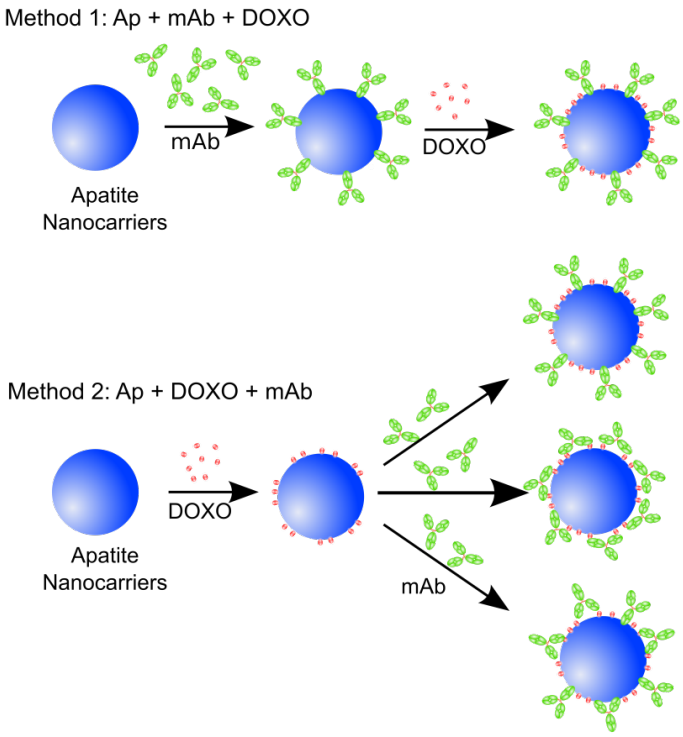

Figure 2. Models of the functionalizing moieties DO-24 mAb and DOXO with Ap nanoparticles according to the two different methods used in this work. Apatite nanocarriers are represented as spheres for clarity, indeed, they are plate-shaped.

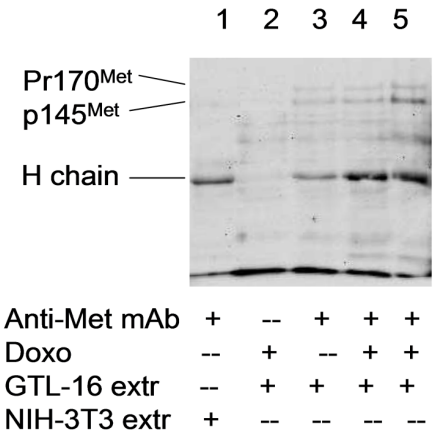

Figure 3. Validation of the immuno-nanoparticles. Binary and ternary Ap nanocrystals were incubated with detergent extracts from GTL-16 (Met^+) cells or NIH-3T3 (Met^-) fibroblasts; unbound proteins were washed away and the remnant was separated in SDS-PAGE, transferred to PVDF paper and processed for western blots with anti-Met antibodies, followed by secondary peroxidase-labelled anti-mouse IgG antibodies. The bands with 145 and 170 kDa, molecular weight, corresponding to Met proteins, could be precipitated only from extracts from cells expressing the Met receptor (GTL-16; lanes 3-5), but not from cells not expressing the Met receptor (NIH-3T3; lane 1) and only if the apatite NPs were loaded with the DO-24 anti-Met mAb (lanes 3-5), thus showing the specificity of mAb loaded NPs. For equivalent amounts of mAb (H chain band), the Ap-mAb-DOXO NPs (lane 5) were more efficient than the Ap-DOXO-mAb NPs (lane 4) in precipitating the Met receptor. For further details see the text. In lanes 2 and 3 ¼ of the immunoprecipitate was loaded.

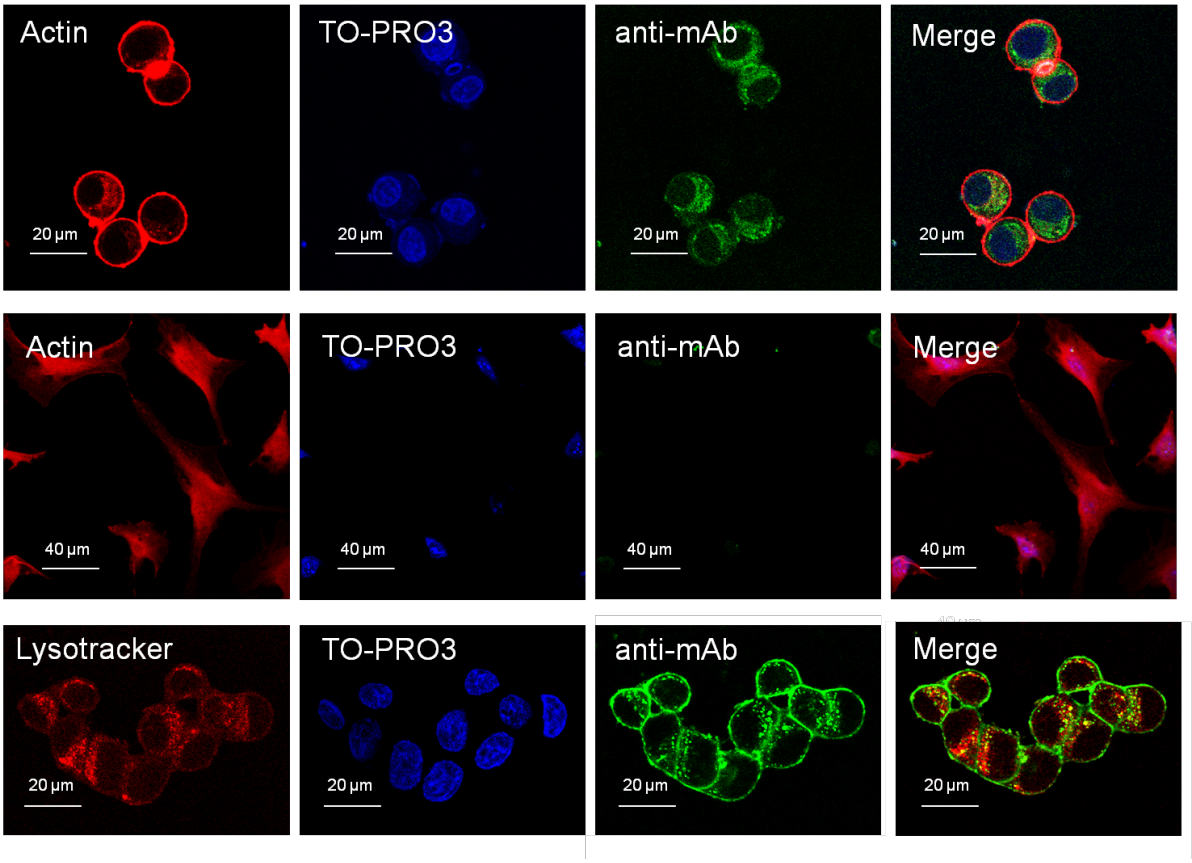

Figure 4. Analysis of the specificity of the interaction of the DO-24 mAb loaded Ap nanoparticles (Ap-mAb) with cells and of their internalization by confocal microscopy. Met^+ GTL-16 cells (top row) and Met^- NIH-3T3 fibroblasts (medium row) were incubated with nanoparticles at 37 °C for 3 h. Fixed and permeabilized treated cells were stained for NPs with FITC-labelled anti-mouse IgG (green), cytoskeletal actin with TRITC-labelled phalloidin (red) and nuclei with TO-PRO3 (blue). mAb-loaded NPs can be detected only in case of GTL-16 cells, but not in case of NIH-3T3 cells, showing the specificity of these nanoparticles. GTL-16 cells incubated with Ap-mAb and lysotracker (botton row, red) were fixed, permeabilized and stained with FITC-labelled anti-mouse IgG (green) and TO-PRO3 (blue). The Ap-mAb nanoparticles co-localize with the Lysotracker-positive endosomal compartment.

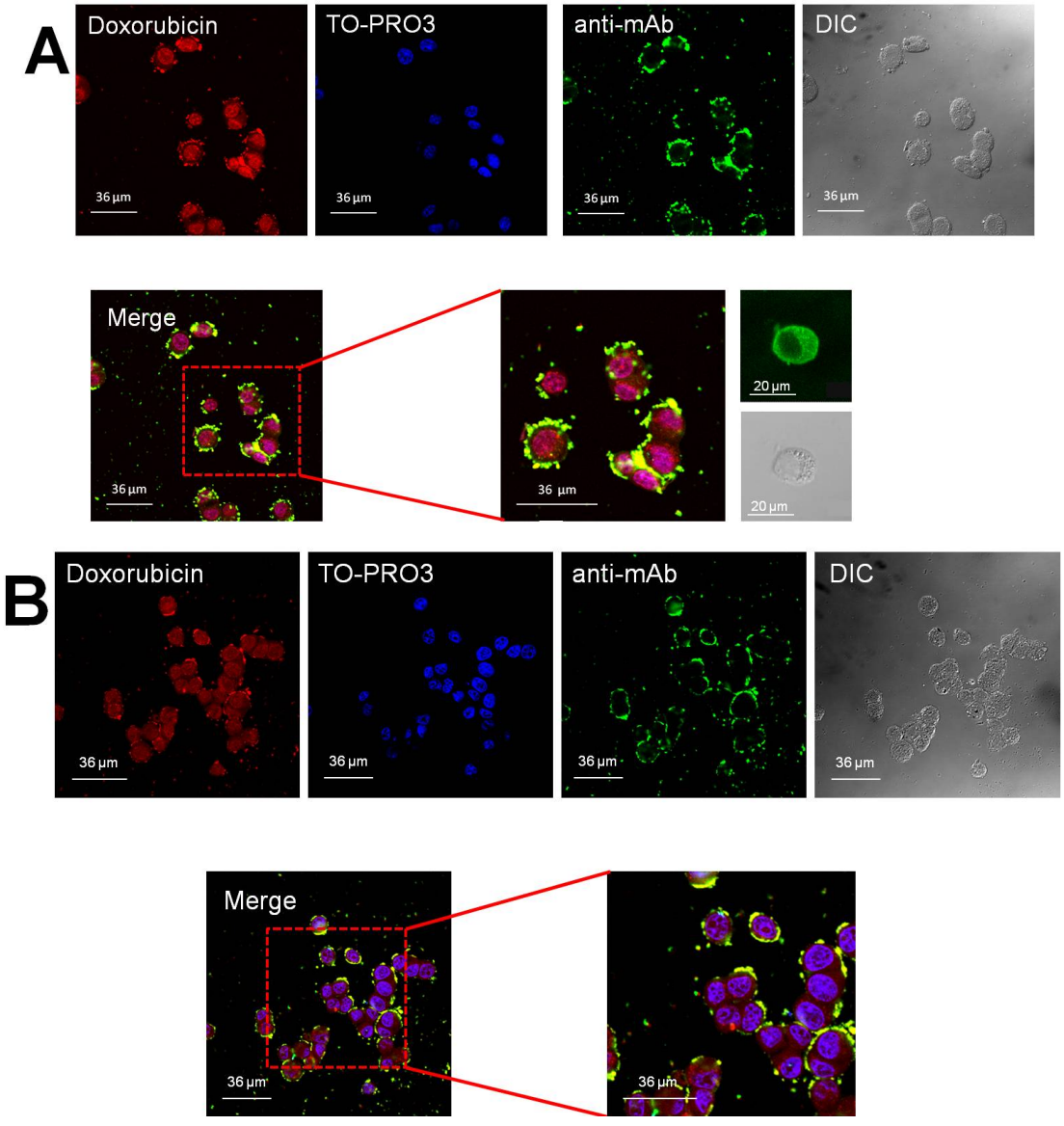

Figure 5. Analysis of the internalization of the ternary nanoparticles in GTL-16 cells by confocal microscopy. Cells were incubated with Ap-mAb-DOXO (A) of Ap-DOXO-mAb (B) nanoparticles at 37°C for 3h, washed, fixed, permeabilized and saturated. Nanoparticles are visualized in green (staining with FITC-labeled anti-mouse IgG), nuclei in blue (TO-PRO3) and DOXO in red. Cell morphology was evaluated in Differential Interference Contrast (DIC)

microscopy. Panel A, bottom right: nanoparticles stained in green can be detected in intracellular vesicles.

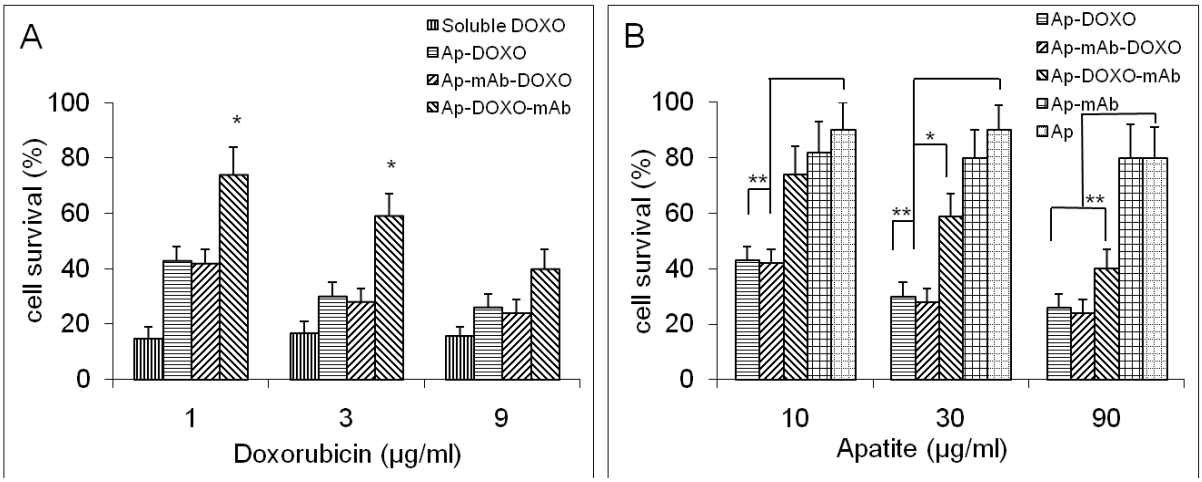

Figure 6. Cytotoxic activity of the differentially functionalized nanoparticles on GTL-16 cells. Cells were incubated with equimolar amounts of DOXO, either soluble or loaded on nanoparticles (A), as well as with equivalent amounts of unfunctionalized nanoparticles (B) for 3 days, before performing the MTT assay. Untreated cells, receiving medium without nanoparticles and DOXO, were taken as reference value (100%) of viable cells to which refer the values of treated cells. Statistical significance: Panel A: ANOVA one-way revealed significant differences ($p<0.001$). Post-hoc test (Sheffè's test) showed highly significant difference in all two-samples comparisons ($p\leq0.001$), except *($p\leq0.05$). Panel B: significance is referred to unfunctionalized nanoparticles (**$p\leq0.001$; *$p\leq0.005$; unlabelled: no significance). Data are the mean ± standard error of the mean (SEM) of 4 experiments performed in triplicates.

Apatite nanoparticles functionalized with the chemotherapeutic doxorubicin and a monoclonal antibody targeting tumor cells overexpressing the tumor associated marker Met/Heaptocyte Growth Factor receptor specifically bind to and are internalized in cells expressing the receptor, and discharge Doxorubicin, which reaches the nucleus and exert cytotoxicity. This work opens new perspectives in the use of nanocrystalline apatites as new platform for theranostic applications in nanomedicine.

M. Iafisco, J. M. Delgado-Lopez, E. M. Varoni, A. Tampieri, L. Rimondini, J. Gomez-Morales, M. Prat*■<B>…<B>■

Cell Surface Receptor Targeted Biomimetic Apatite Nanocrystals for Cancer Therapy

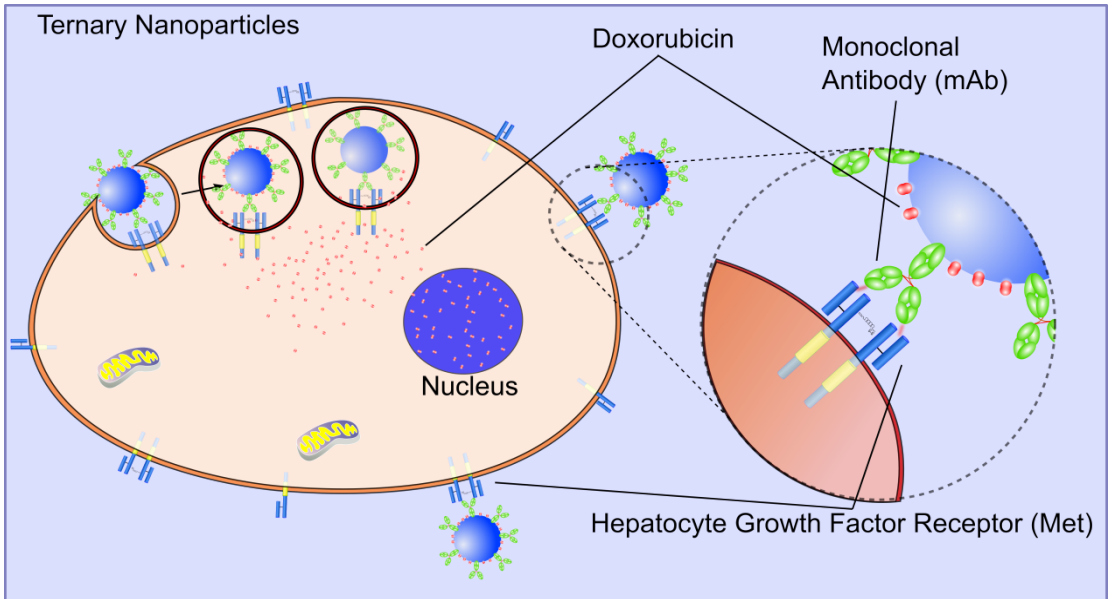

Page Headings
Left page: Iafisco et al.
Right page: Targeted Apatite Nanocrystals for Cancer Therapy